Defence Science Journal, Vol. 64, No. 6, November 2014, pp. 564-570, DOI : 10.14429/dsj.64.4747

Amplitude and Phase Statistics of Multi-look SAR Complex Interferogram

Yu Anxi*, Wei Haijun#, Dong Zhen, and Huang Haifeng

National University of Defense Technology, Changsha-410 073, China
#Naval Equipment Technology Institute, Beijing-102 442, China
**E-mail: yu_anxi@sina.com*

ABSTRACT

Amplitude and phase statistics of SAR complex interferogram are significant in the study of interferometry and polarimetry. To reduce statistical variations, multi-look processing is adopted by averaging spatially the complex interferogram. In this study, we derive and validate three kinds of probability density functions (PDFs) of multi-look interferogram for different surface feature scenes. For simple homogeneous areas with the gamma distribution intensity, a concise product-form interferometry phase PDF is derived, which is equivalent to a conventional Gauss hypergeometric PDF. For complicated areas with the K and G^0 distributions intensity, two new interferometry amplitude PDFs named as Gamma-K and Gamma-G are proposed, and their phase PDFs are approximately preserved. Finally three typical areas including grass, mountain, and city are picked out from a pair of RADARSAT-2 SAR images and studied. Experimental results indicate good agreement between the computed histograms and the theoretical distributions. The results obtained can be applied to the feature classification of polarisation SAR data and the estimation of decorrelation effect of interferometric SAR.

Keywords: Synthetic aperture radar, complex interferogram, amplitude and phase statistics, probability density functions

1. INTRODUCTION

Amplitude and phase statistics of SAR complex interferogram are significant in the study of interferometry and polarimetry. SAR complex interferogram is widely applied in many technology fields, such as interferometry measure[1], interferometry SAR signal simulation[2], move target detection[3,4], polarimetric interferometry[5,6,7], building edge detection[8], polarimetric SAR image segmentation[9], water change detection[10]. Usually these distribution models are established by statistically deducing amplitude and phase PDFs after analyzing statistic characteristics of SAR complex interferogram. In the past for the demands of understanding synthetic aperture radar images, the clutter intensity distribution was widely concerned. Several clutter intensity probability distribution models have been proposed for different scenes, such as Gamma distribution[11], K distribution[12] and G^0 distribution[13]. Since 1993, the statistics study of the interferometry phase took an important progress. Bamler and Just[14,15] analyzed quantitatively the influence of decorrelation on the phase statistics of SAR interferograms, discussed the probability density function of the interferometric phase for arbitrary transfer functions, and pointed out that the phase statistics are completely determined by the complex correlation coefficient. Tough[16], *et al.* provided an analysis of the key distributions encountered in single and multi-look polarimetric and interferometric SAR data, under a Gaussian or multi-variate K distribution model. In the same year, for simple homogeneous scene whose intensity is characterised as Gamma distribution, Lee[17,18], *et al.* derived PDFs of the multi-look phase difference, magnitude of complex product, and intensity and amplitude ratios between two components of the scattering matrix from the complex Wishart distribution and pointed out the multi-look phase difference has a Gauss hypergeometric distribution, and the multi-look amplitude distribution is a product of two modified Bessel functions. The procedures involve multiple integrations of special functions, thus yielding closed-form, easily computable solutions for the PDFs. All these results laid a foundation for SAR interferometry and polarimetry research.

With the development of SAR interferometry and polarimetry technology, more accurate amplitude and phase statistical models of SAR complex interferogram need be established for different complicated scenes, such as grass, mountain and city. Usually the clutter statistics in the grass area is adjacent to Gamma distribution, and mountain and city are usually different. The clutter PDF of complicated scene is usually established as the K or G^0 distribution model for the heavy tail characteristic[12,13]. Gui[19], *et al.* developed a joint distribution of magnitude and phase for multi-look SAR interferogram in extremely heterogeneous clutter, the model performance was validated on two dual-channel SAR images. Recently, a novel distribution denoted as S^1 distribution was proposed for modelling the textural component[20].

2. STATISTICAL MODELS OF SAR CLUTTER INTENSITY

2.1 Simple Homogeneous Scene

As we know, SAR speckle noise is severer in higher intensity areas, which is fitted to the multiplicative model[21]. Full growth speckle noise hypothesis is usually satisfied for the simple homogeneous scene. The SAR image intensity can

Received 25 July 2013, revised 28 August 2014, online published 13 November 2014

be represented as the product of the RCS background and the speckle noise as follows:

$$I(a,r)=\sigma(a,r)\cdot\omega(a,r) \tag{1}$$

where a and r represent the azimuth and range position respectively, and σ isn't related to ω.

For simple homogeneous scene, the RCS background $\sigma(a,r)$ can be looked as a constant. Multi-look clutter intensity of the SAR image has a Gamma distribution[11] as follows:

$$p(I)=\frac{n^n I^{n-1}}{\left(\bar{I}\right)^n \Gamma(n)} e^{\left(-\frac{nI}{\bar{I}}\right)} \tag{2}$$

where $E[I]=\bar{I}$, n is the number of looks, and $\Gamma(\cdot)$ is the Gamma function.

2.2 Complicated Scene

For some complicated scenes, $\sigma(a,r)$ can't be treated as a constant, so some new clutter probability distribution models need be derived.

(1) *K distribution clutter intensity statistical model*

Suppose $\sigma(a,r)$ has a Gamma distribution as follows:

$$p_K(\sigma)=\frac{L^L\sigma^{L-1}}{(\bar{\sigma})^L\Gamma(L)} e^{\left(-\frac{L\sigma}{\bar{\sigma}}\right)} \tag{3}$$

where L is a model parameter, and $\bar{\sigma}$ is the mean of the RCS. Thus the multi-look clutter intensity has a K distribution statistical model as follows:

$$p_K(I)=\frac{2}{\Gamma(L)\Gamma(n)}(\lambda L)^{(L+n)/2} I^{(L+n-2)/2} K_{n-L}\left[2(\lambda L I)^{1/2}\right] \tag{4}$$

where $\lambda=n/\bar{\sigma}$, and $K_n[\cdot]$ is the third kind of modified Bessel function.

(2) *G^0 distribution clutter intensity statistical model*

Suppose $\sigma(a,r)$ has an inverse Gamma distribution as follows:

$$p_{G^0}(\sigma)=\frac{2}{\gamma^{\kappa}\Gamma(-\kappa)}\sigma^{\kappa-1}e^{\frac{\gamma}{\sigma}} \tag{5}$$

where κ ($\kappa<0$) and γ is two model parameters. Thus the multi-look clutter intensity has a G^0 distribution statistical model as follows:

$$p_{G^0}(I)=\frac{n^n\Gamma(n-\kappa)I^{n-1}}{\gamma^{\kappa}\Gamma(n)\Gamma(-\kappa)(\gamma+nI)^{n-\kappa}} \tag{6}$$

3. STATISTICAL MODELS OF INTERFEROGRAM AMPLITUDE AND PHASE

3.1 The Expression of Multi-look Interferogram

Let v_1 and v_2 denote the master and slave SAR images, and then

$$\begin{cases} v_1(k)=\sqrt{\sigma_1(k)}\cdot u_1(k) \\ v_2(k)=\sqrt{\sigma_2(k)}\cdot u_2(k) \end{cases} \tag{7}$$

where k denotes the pixel position, which is sometimes ignored in the following text. u_1 and u_2 are two correlative normalised complex noises with a circular Gaussian density function[22] and $E[u_1u_1^*]=E[u_2u_2^*]=1$. σ_1 and σ_2 represent the RCS textures. u and σ are commonly assumed to be independent. The multi-look complex interferogram may be written as follows:

$$He^{j\psi}=\frac{1}{n}\sum_{k=1}^{n}v_1(k)v_2^*(k)=\frac{1}{n}\sum_{k=1}^{n}\sigma(k)u_1(k)u_2^*(k) \tag{8}$$

where H and ψ are the amplitude and phase of interferogram, and n is the number of looks. In next section, three statistical models of $\sigma(k)$ are discussed and applied to deduce the statistical distributions of the interferogram.

- $\sigma(k)$ is a constant, the scene is simple homogeneous.
- $\sigma(k)$ has a Gamma density function, the scene is more complicated.
- $\sigma(k)$ has an inverse Gamma density function, the scene is extremely heterogeneous.

3.2 Statistical Models of Interferogram Amplitude and Phase for Simple Scene

Suppose that

$$A=\sum_{k=1}^{n}\begin{bmatrix}v_1(k)\\ v_2(k)\end{bmatrix}\begin{bmatrix}v_1(k)^* & v_2(k)^*\end{bmatrix}=\begin{bmatrix}A_{11} & nHe^{j\psi}\\ nHe^{-j\psi} & A_{22}\end{bmatrix}=\begin{bmatrix}A_{11} & A_{12}\\ A_{21} & A_{22}\end{bmatrix} \tag{9}$$

Complex correlation coefficient between two SAR images is

$$\rho e^{j\theta}=\frac{E\left[v_1v_2^*\right]}{\sqrt{E\left[|v_1|^2\right]E\left[|v_2|^2\right]}} \tag{10}$$

The complex covariance matrix is

$$\mathbf{C}=\begin{bmatrix}E\left[v_1v_1^*\right] & E\left[v_1v_2^*\right]\\ E\left[v_2v_1^*\right] & E\left[v_2v_2^*\right]\end{bmatrix}=\begin{bmatrix}C_{11} & \sqrt{C_{11}C_{22}}\rho e^{j\theta}\\ \sqrt{C_{11}C_{22}}\rho e^{-j\theta} & C_{22}\end{bmatrix} \tag{11}$$

For the simple homogeneous scene is with a constant $\sigma(k)$, the matrix $\mathbf{A}$ has a complex Wishart distribution[17]

$$p(\mathbf{A})=\frac{\det(\mathbf{A})^{n-2}}{\pi\Gamma(n)\Gamma(n-1)\det(\mathbf{C})^n}\exp\left(-tr\left\{\mathbf{C}^{-1}\mathbf{A}\right\}\right) \tag{12}$$

After some simplifications, the joint PDF of interferogram amplitude and phase are derived, which is a Gauss hypergeometric model as follows:

$$p(\eta,\psi)=\frac{2n^{n+1}\eta^n}{\pi\cdot\Gamma(n)(1-\rho^2)}\cdot\exp\left(\frac{2n\eta\rho\cos(\psi-\theta)}{1-\rho^2}\right)K_{n-1}\left(\frac{2n\eta}{1-\rho^2}\right) \tag{13}$$

where $\eta=H/\sqrt{C_{11}C_{22}}$ is the normalised multi-look interferogram amplitude.

$$\eta=\frac{\left|\frac{1}{n}\sum_{k=1}^{n}\sigma(k)u_1(k)u_2^*(k)\right|}{\sqrt{E\left[v_1v_1^*\right]E\left[v_2v_2^*\right]}}=\frac{\left|\frac{\sigma}{n}\sum_{k=1}^{n}u_1(k)u_2^*(k)\right|}{\sigma}=\left|\frac{1}{n}\sum_{k=1}^{n}u_1(k)u_2^*(k)\right| \tag{14}$$

Integration of Eqn. (13) wrt ψ and using the above equation, yields the IK distribution model of the normalised multi-look interferogram amplitude as follows:

$$p_{\eta}(\eta)=\frac{4n^{n+1}\eta^n}{\Gamma(n)\left(1-\rho^2\right)}I_0\left(\frac{2\rho n\eta}{1-\rho^2}\right)K_{n-1}\left(\frac{2n\eta}{1-\rho^2}\right) \tag{15}$$

where $I_0(\bullet)$ is the modified Bessel function of order zero.

Similarly the phase distribution can be obtained by integrating Eqn (13) with respect to amplitude η.

$$p(\psi)=\frac{2n^{n+1}}{\pi\cdot\Gamma(n)(1-\rho^2)}\cdot\int_0^\infty \eta^n \exp(\frac{2n\eta\rho\cos(\psi-\theta)}{1-\rho^2})\mathrm{K}_{n-1}(\frac{2n\eta}{1-\rho^2})d\eta \tag{16}$$

Let $p=-2n\rho\cos(\psi-\theta)/(1-\rho^2)$, and $c=2n/(1-\rho^2)$, we have

$$p(\psi)=\frac{2n^{n+1}}{\pi\cdot\Gamma(n)(1-\rho^2)}\cdot\int_0^\infty \eta^n \exp(-p\eta)\mathrm{K}_{n-1}(c\eta)d\eta \tag{17}$$

Notice $p+c>0$ and apply the second integration expression of the Eqns (2.16.6.3) in the Frery[23], *et al.* one gets a product-form PDF of interferogram phase as follows

$$p(\psi)=\frac{(1-\rho^2)^n\,\Gamma(2n)}{2\sqrt{\pi}\Gamma(n)\Gamma(n+1.5)(1-\rho\cos(\psi-\theta))^{2n}}\,{}_2F_1\left(n-\frac{1}{2},2n;n+\frac{3}{2};\frac{\rho\cos(\psi-\theta)+1}{\rho\cos(\psi-\theta)-1}\right) \tag{18}$$

where ${}_2F_1(\bullet)$ is the Guass hypergeometric function.

A hypergeometric PDF model of interferogram phase derived by Lee[17], *et al*. is

$$p(\psi)=\frac{\Gamma(n+1/2)(1-\rho^2)^n\,\rho\cos(\psi-\theta)}{2\sqrt{\pi}\Gamma(n)(1-\rho^2\cos^2(\psi-\theta))^{(n+1/2)}}+\frac{(1-\rho^2)^n}{2\pi}\,{}_2F_1(n,1;1/2;\rho^2\cos^2(\psi-\theta)) \tag{19}$$

The equivalence relation between Eqns. (18) and (19) can be proven by mathematic software. We can see that new formula Eqn. (18) has a more concise product form than conventional formula Eqn. (19).

3.3 Statistical Models of Interferogram Amplitude and Phase for Complicated Scenes

Suppose the scattering texture is approximately constant in the local multi-look window area, the Eqn. (8) can be written as

$$He^{j\psi}=\frac{1}{n}\sum_{k=1}^{n}v_1(k)v_2^*(k)=\frac{1}{n}\sum_{k=1}^{n}\sigma(k)u_1(k)u_2^*(k)=\frac{\sigma}{n}\sum_{k=1}^{n}u_1(k)u_2^*(k) \tag{20}$$

Regarding the clutter intensity statistical model as *K* distribution or G^0 distribution for complicated scene, the corresponding image scattering texture σ_1 and σ_2 are independent and real random variables with the Gamma function or inverse Gamma function distributions.

One can see that the interferogram phase is unrelated to σ, so the former interferogram phase statistical model is also applicable to the complicated scene.

Referring to Eqn. (20), the interferogram amplitude *H* is

$$H=\left|\frac{\sigma}{n}\sum_{k=1}^{n}u_1(k)u_2^*(k)\right|=\sigma\cdot\left|\frac{1}{n}\sum_{k=1}^{n}u_1(k)u_2^*(k)\right|=\sigma\cdot\eta \tag{21}$$

So the interferogram amplitude *H* can be regarded as the product of a real random variable σ and the normalized multi-look interferogram amplitude η of simple homogeneous scene.

Case (1): When σ has a Gamma distribution function as Eqn.(3), the PDF of the interferogram amplitude *H* is

$$p_K(H)=\int_0^\infty\frac{1}{\sigma}p_\eta(H/\sigma)p_K(\sigma)d\sigma \tag{22}$$

Substitute Eqn. (3) and Eqn. (15) into Eqn. (22) yields

$$p_K(H)=\int_0^\infty\frac{4n^{n+1}H^n}{\Gamma(n)(1-\rho^2)\sigma^{n+1}}\frac{\lambda^L L^L\sigma^{L-1}}{n^L\Gamma(L)}e^{\left(-\frac{L\sigma\lambda}{n}\right)}I_0\left(\frac{2\rho nH/\sigma}{1-\rho^2}\right)K_{n-1}\left(\frac{2nH/\sigma}{1-\rho^2}\right)d\sigma$$

$$=\frac{4n^{n+1}H^n}{\Gamma(n)(1-\rho^2)}\frac{\lambda^L L^L}{n^L\Gamma(L)}\int_0^\infty\sigma^{L-n-2}e^{\left(-\frac{L\sigma\lambda}{n}\right)}I_0\left(\frac{2\rho nH/\sigma}{1-\rho^2}\right)K_{n-1}\left(\frac{2nH/\sigma}{1-\rho^2}\right)d\sigma \tag{23}$$

Case (2): When σ has an inverse Gamma distribution function as Eqn. (5), we have

$$p_{G^0}(H)=\int_0^\infty\frac{1}{\sigma}p_\eta(H/\sigma)p_{G^0}(\sigma)d\sigma \tag{24}$$

Substitute Eqn. (5) and Eqn. (15) into Eqn. (22) yields

$$p_{G^0}(I)=\int_0^\infty\frac{4n^{n+1}H^n}{\Gamma(n)(1-\rho^2)\sigma^{n+1}}\frac{2}{\gamma^\kappa\Gamma(-\kappa)}\sigma^{\kappa-1}e^{\frac{\gamma}{\sigma}}I_0\left(\frac{2\rho nH/\sigma}{1-\rho^2}\right)K_{n-1}\left(\frac{2nH/\sigma}{1-\rho^2}\right)d\sigma$$

$$=\frac{4n^{n+1}H^n}{\Gamma(n)(1-\rho^2)}\frac{2}{\gamma^\kappa\Gamma(-\kappa)}\int_0^\infty\sigma^{\kappa-n-2}e^{\frac{\gamma}{\sigma}}I_0\left(\frac{2\rho nH/\sigma}{1-\rho^2}\right)K_{n-1}\left(\frac{2nH/\sigma}{1-\rho^2}\right)d\sigma \tag{25}$$

here, the expressions Eqns (23) and (25) are the statistic distribution models of the complex interferogram respectively for the K and G^0 distribution clutter scenes, which are named by the authors as Gamma-K and Gamma-G distribution models, respectively.

4. MODELS VALIDATION WITH THE REAL DATA

A pair of RADARSAT-2 SAR images acquired on 4th May and 28th May 2008 over Toronto was used to validate the above theoretical models. The master image is showed as Fig. 1, in which three representative areas are picked out and denoted as A (grass), B (plain mountain), and C (city), respectively.

4.1 Validation of the Clutter Statistic Models

The clutter intensity of the three types of areas is respectively fitted to Gamma, *K*, and G^0 distribution models, and the model parameters are obtained by moment estimation method in the Baselice & Ferraioli[8]. The estimated model parameters of the selected areas in the master and slave images are given as Table 1, Table 2, and Table 3, and the corresponding fitted PDFs of the intensity are showed in Figs 2, 3, and 4. The fitted error ε is computed as the difference of the real data and the fitted model.

$$\varepsilon=\sum_{i=1}^{N}\left(p(x_i)-y_i\right)^2 \tag{26}$$

where *N* denotes the number of the image intensity partitions, y_i denotes the proportion of the i-th partition, and $p(x_i)$ denotes the fitted PDF. It was found that the Gamma distribution intensity model is distinctly superior for the grass and plain mountain areas, which has fewer model parameters and higher

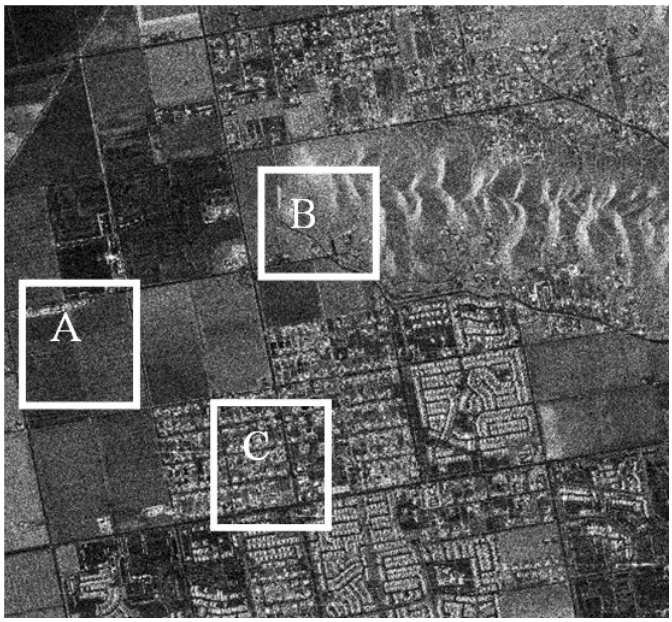

Figure 1. The master image and three experimental areas (A: grass; B: plain mountain; C: city).

accuracy. For the city area, the G^0 distribution intensity model is the best one, and the K distribution model follows.

4.2 Validation of Interferogram Phase Statistic Model

The parameter ρ of the model Eqn. (18) is chosen as the mean correlation coefficient of the three areas, and n is estimated by function fitting. Table 4 shows the estimated model parameters of the interferogram phase in different experiment areas. We can see that all the fitted errors are enough low for

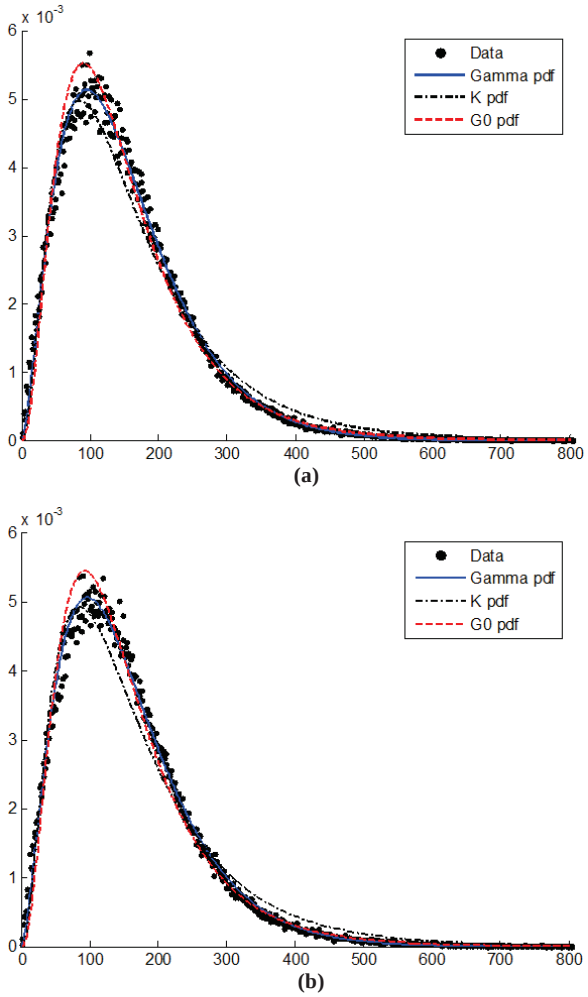

Figure 2. The fitted intensity PDFs in areas A(grass) : (a) The master image, and (b) The slave image.

Table 1. The estimated model parameters of intensity distribution in area A (grass)

	Gamma		K				G^0			
	n	ε	n	L	λ	ε	n	γ	κ	ε
Master image	2.650	0.043	4.433	4.224	0.026	0.093	3.371	1586	-11.342	0.065
Slave image	2.660	0.041	4.408	4.224	0.026	0.101	3.407	1658	-11.649	0.068

Table 2. The estimated model parameters of intensity distribution in area B (plain mountain)

	Gamma		K				G^0			
	n	ε	n	L	λ	ε	n	γ	κ	ε
Master image	2.880	0.029	4.502	4.220	0.016	0.071	3.562	3056	-13.443	0.049
Slave image	2.890	0.034	4.540	4.218	0.015	0.083	3.505	3493	-13.926	0.057

Table 3. The estimated model parameters of intensity distribution in area C (city)

	Gamma		K				G^0			
	n	ε	n	L	λ	ε	n	γ	κ	ε
Master image	1.800	0.062	3.774	4.129	0.012	0.031	2.524	1446	-5.499	0.021
Slave image	1.820	0.087	3.784	4.135	0.012	0.044	2.567	1536	-5.613	0.031

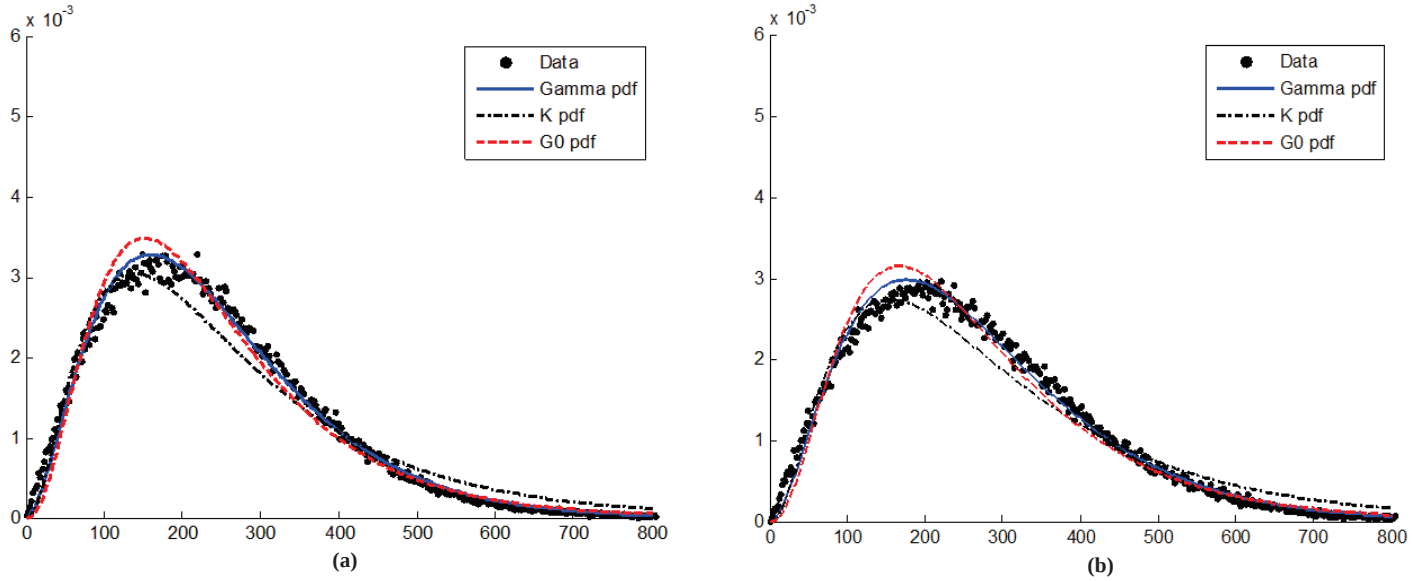

Figure 3. The fitted intensity PDFs in area B (plain mountain): (a) The master image, and (b) The slave image.

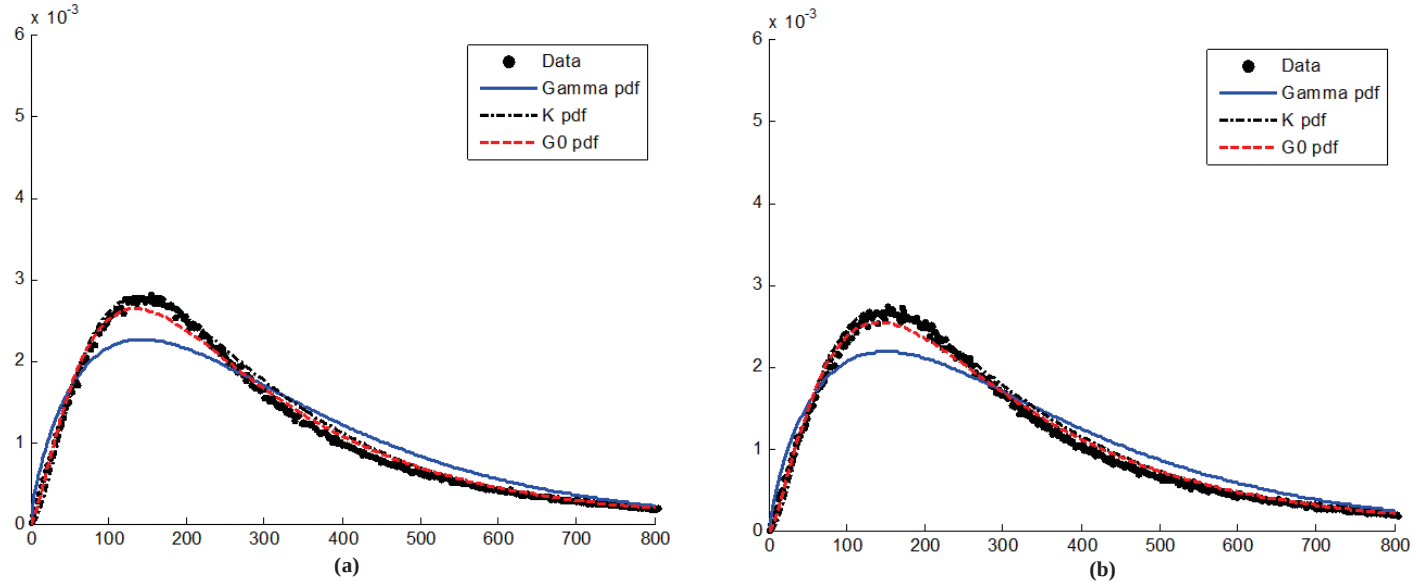

Figure 4. The fitted intensity PDFs in area C (city): (a)The master image, and (b) the slave image.

the three scenes. That is to say, Eqn. (18) is a universal PDF model for all scenes.

4.3 Validation of Interferogram Amplitude Statistic Model

For describing the statistical models of interferogram amplitude Eqns (15), (23), and (25), the above estimated parameters in Sections 4.1 and 4.2 are used. There into, the parameter ρ is chosen as the mean correlation coefficient of the three areas. The parameters L and λ in Eqn. (23) are chosen as the averages of the estimated K distribution model parameters of the master and slave images in Table 1, Table 2, and Table 3. The parameters γ and λ in Eqn. (25) are averages of the estimated G^0 distribution model parameters of the master and slave images in Table 1, Table 2, and Table 3. The parameter n is estimated by function fitting. The estimated PDF model

Table 4. The estimated model parameters and errors of the interferogram phase

Area A			Area B			Area C		
ρ	n	ε	ρ	n	ε	ρ	n	ε
0.749	2.315	0.018	0.636	2.731	0.021	0.491	2.524	0.024

Table 5. The estimated PDF model errors of the interferogram amplitude

	Fitted model errors		
	IK	Gamma-K	Gamma-G
Area A	0.049	0.031	0.036
Area B	0.219	0.035	0.050
Area C	0.191	0.187	0.118

errors of the interferogram amplitude and the fitted PDF curves in the different experiment areas are respectively showed in Table 5 and Figure 5.

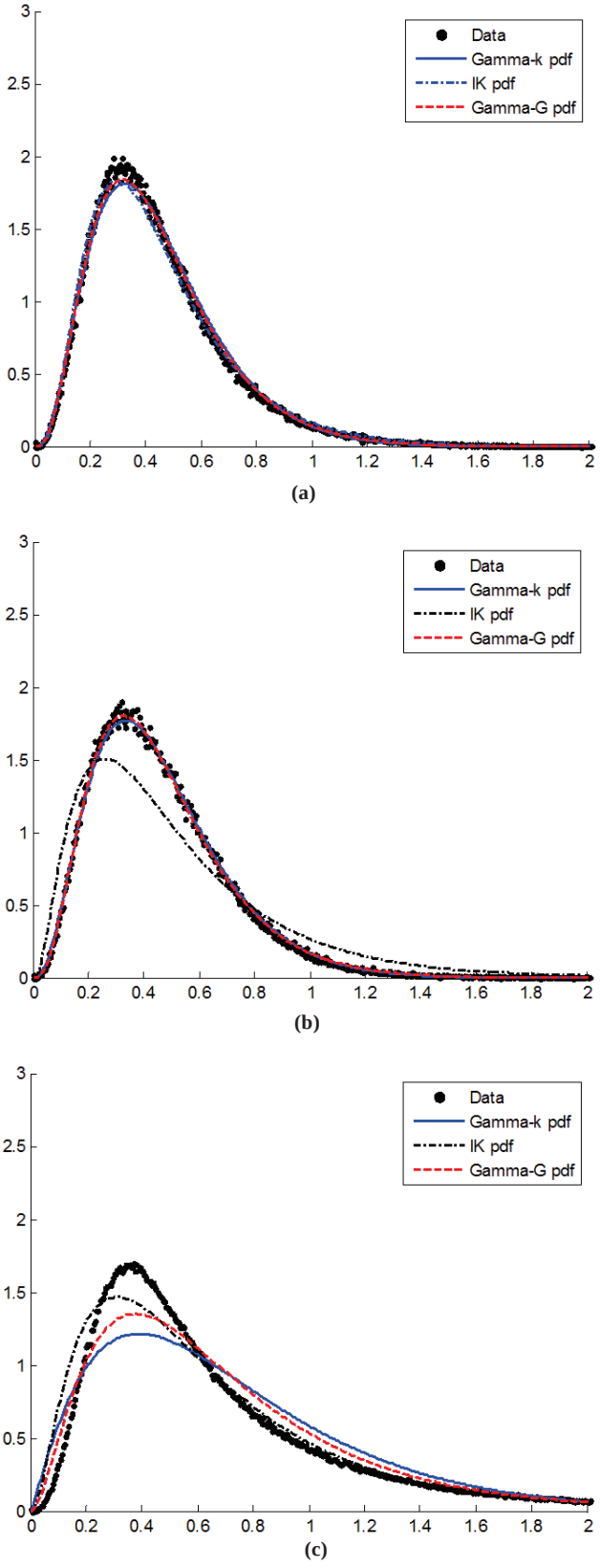

Figure 5. Fitted PDF curves of interferogram amplitude in different experimental areas (a) Area A: grass, (b) Area B: plain mountain, and (c) Area C: city.

5. CONCLUSIONS

Following conclusions have been drawn:

- All the three models have perfect results for the grass area.
- For the plain mountain area, Gamma-K and Gamma-G distribution models are all feasible, and IK model has higher errors.
- For the city area, three models are all unperfect for the potential reason of more dot-scattering characteristic, especially IK model has the worst fitted results, and only Gamma-G model is almost acceptable.

In this, research the authors have derived and validated three kinds of probability density functions (PDFs) of multi-look interferogram for the different surface feature scenes. For simple homogeneous areas with the Gamma distribution intensity, a concise product-form interferometry phase PDF has been derived, which is equivalent to a conventional Gauss hypergeometric PDF. For complicated areas with the *K* and G^0 distributions intensity, two new interferometry amplitude PDFs named as Gamma-K and Gamma-G are proposed, and their phase PDFs are approximately preserved. Experimental results indicate good agreements between the histograms and all the theoretical distributions. The results of this paper can be applied to the feature classification of polarisation SAR data and the estimation of decorrelation effect of interferometric SAR.

ACKNOWLEDGEMENT

This research was supported by the National Natural Science Foundation of China (NSFC) under Grants 61002031 and 60903206.

REFERENCES

1. Xu, H.P. & Kang, C.H. Equivalence analysis of accuracy of geolocation models for space-borne InSAR. *IEEE Trans. Geosci. Remote Sens.*, 2010, **48**(1), 480-490. doi: 10.1109/TGRS.2009.2027897
2. Lu, X.Q. Study on modeling and simulation of distributed space-borne InSAR. National University of Defense Technology, Changsha, China, 2006. PhD Thesis.
3. Gierull, C.H. Statistical analysis of multi-look SAR interferograms for CFAR detection of ground moving targets. *IEEE Trans. Geosci. Remote Sens.*, 2004, **42**(4), 691-701. doi: 10.1109/TGRS.2003.821886
4. Gao, G. & Shi, G. The CFAR detection of ground moving targets based on a joint metric of SAR interferogram's magnitude and phase. *IEEE Trans. Geosci. Remote Sens.*, 2012, **50**(9), 3618-3624. doi: 10.1109/TGRS.2012.2184836
5. Ferro-Famil, L. & Neumann, M. Recent advances in the derivation of Pol-InSAR statistics: Study and applications. EUSAR, 2008, VDE, 1-4.
6. Tough, R. J. A.; Blacknell, D. & Quegan, S. A statistical description of polarimetric and interferometric synthetic aperture radar data. *In* Proceedings of the Royal Society of London. Series A: Mathematical and Physical Sciences, 1995, **449**(1937), 567-589.
7. Roueff, A. & Arnaubec, A. Cramer–Rao lower bound

analysis of vegetation height estimation with random volume over ground model and polarimetric SAR interferometry. *IEEE Geosci. Remote Sens. Let.,* 2011, **8**(6), 1115-1119. doi: 10.1109/LGRS.2011.2157891

8. Baselice, F. & Ferraioli, G. Statistical edge detection in urban areas exploiting SAR complex data. *IEEE Geosci. Remote Sens. Letters,* 2012, **9(**2), 185-189. doi: 10.1109/LGRS.2011.2163295
9. Chaudhuri, Sanjay D.; Singh, M.P. & Mishra, A. An adaptive seed point selection technique for segmentation of polarimetric synthetic aperture radar image. *In* Proceedings of IEEE Second International Conference of Image Information Processing (ICIIP), 2013, 21-26.
10. Zhi, Liu; Lingyan, Chen; Chao, Wang & Lei, Xie. Water change detection based on complex Wishart distribution model using polarimetric SAR image. EUSAR 2014, 10th Proceedings of European Conference on Synthetic Aperture Radar, 1-4, June 2014.
11. Goodman, J.W. Statistical properties of laser speckle patterns. Laser speckle and related phenomena. Springer Berlin Heidelberg, 1975, **9**, pp.9-75. doi: 10.1007/BFb0111436
12. Jakeman, E. & Pusey, P. A model for non-Rayleigh sea echo. *IEEE Trans. Anten. Propag.,* 1976, **24**(6), 806-814. doi: 10.1109/TAP.1976.1141451
13. Frery, A.C.; Muller, H.J.; Yanasse, C.C.F. & Sant'Anna, S.J.S. A model for extremely heterogeneous clutter. *IEEE Trans. Geosci. Remote Sens.,* 1997, **35**(3), 648-659. doi: 10.1109/36.581981
14. Bamler, R. & Just, D. Phase statistics and decorrelation in SAR interferograms. *IEEE Geosci. Remote Sens. Symp.,* 1993, 980-984.
15. Just, D. & Bamler, R. Phase statistics of interferograms with applications to synthetic aperture radar. *Applied Optics,* 1994, **33**(20), 4361-4368. doi: 10.1364/AO.33.004361
16. Tough, R. J. A.; Blacknell, D. & Quegan, S. Estimators and distributions in single and multi-look polarimetric and interferometric data. *IEEE Geosci. Remote Sens. Symp.,* 1994, **4**, 2176-2178.
17. Lee, J.S.; Miller, A.R. & Hoppel, K.W. Statistics of phase difference and product magnitude of multi-look processed Gaussian signals. *Waves in Random Media,* 1994, **4**(3), 307-319. doi: 10.1088/0959-7174/4/3/006
18. Lee, J.S.; Hoppel, K.W. & Mango, S.A. Intensity and phase statistics of multi-look polarimetric and interferometric SAR imagery. *IEEE Trans. Geosci. Remote Sens.,* 1994, **32**(5), 1017-1028. doi: 10.1109/36.312890
19. Gui G.; Shi, G. & Zhou, S. Modeling Multi-look Magnitude and Phase in Extremely Heterogeneous Clutter. *Int. J. Antennas Propag.*, 2013, **2013,** pp1-5. doi:10.1155/2013/468380
20. Qin, Xianxiang; Zhou, Shilin; Zou, Huanxin & Gao, Gui. Statistical modelling of a joint metric of SAR interferogram's magnitude and phase using Fisher distribution for texture. In IOP Conference Series: Earth and Environmental Science, 2014, **17**, conference 1. doi:10.1088/1755-1315/17/1/012248
21. Goodman, J.W. Some fundamental properties of speckle, JOSA, 1976, **66**(11), 1145-1150. doi: 10.1364/JOSA.66.001145
22. Goodman, N.R. Statistical analysis based on certain multivariate complex Gaussian distribution. *Ann. Mathe. Statis.,* 1963, **34**(1), 152-177. doi: 10.1214/aoms/1177704250
23. Prudnikov, A.P.; Brychkov I.A. & Marichev, O.I. Integrals and series: special functions, Vol. 2. Taylor & Francis, 1986.

CONTRIBUTORS

Dr Yu Anxi received PhD from National University of Defense Technology in 2003. He is currently an Associate Professor with the College of Electronic Science and Engineering, National University of Defense Technology. His current research interests include SAR geocoding, interferometry SAR and differential interferometry SAR.

Dr Wei Haijun received PhD from National University of Defense Technology in 2011. He is currently an engineer with the Naval Equipment Technology Institute. His current research interests include interferometry SAR and equipment fault diagnosis.

Dr Dong Zhen received the PhD from National University of Defense Technology in 2001. He is currently a Professor with the College of Electronic Science and Engineering, National University of Defense Technology. His recent research interests include SAR system design and processing, interferometry SAR, and digital beamforming.

Dr Huang Haifeng received the PhD from National University of Defense Technology in 2005. He is currently an Associate Professor with the College of Electronic Science and Engineering, National University of Defense Technology. His current research interests include SAR system design and processing, interferometry SAR.